Online Magnetization Trajectory Prediction and Current Control for a Variable-Flux Permanent Magnet Machine

JUNHUA CHEN, (Member, IEEE), HAIYANG FANG, (Member, IEEE), AND RONGHAI QU, (Fellow, IEEE)

State Key Laboratory of Advanced Electromagnetic Engineering and Technology, School of Electrical and Electronic Engineering, Huazhong University of Science and Technology, Wuhan 430074, China

Corresponding author: Haiyang Fang (haiyangfang@hust.edu.cn)

ABSTRACT Online magnetization current control is a critical concern of the variable-flux permanent magnet machine control. Increasing the magnetization speed benefits the machine system, which reduces manipulation losses and mechanical impact. Thus, this paper proposes an online trajectory prediction method that increases the DC-link voltage utilization, boosting the manipulation speed. The prediction method decouples the rotating voltage and the induction voltage in the machine model. The induction voltage is the source of di/dt, which influences the magnetization manipulation speed. The proposed method updates the maximum available induction voltage at every manipulation stage by excluding the rotating voltage from the DC-link voltage limitation. Based on the induction voltage, the magnetization current trajectory is predicted. The trajectory prediction is cooperated with a feed-forward current controller to increase the control dynamics. Verified by various experiments, the proposed method achieves fast manipulation speed with high control accuracy. Besides, the proposed method shows self-adaptive capabilities in variable-speed and variable-voltage conditions.

INDEX TERMS Current control, feed-forward PI controller, magnetization, mathematical model, motor control, variable-flux permanent magnet machine.

I. INTRODUCTION

Variable speed applications like electric vehicles require high-efficiency electric machine systems. Permanent magnet synchronous machines (PMSMs) are one of the major machine types being applied in the variable speed fields [1], [2]. Although the rotor flux in the PMSMs is generated by the permanent magnets, flux-weakening current is necessary when the rotor back electromotive-force (EMF) surpasses the DC-link voltage limitation. The flux-weakening current creates addition losses and damages the overall efficiency of the machine system.

Variable-flux permanent magnet machines (VFPMs) or memory machines have been proposed to eliminate the continuous flux-weakening current [3], [4]. The VFPMs use

The associate editor coordinating the review of this manuscript and approving it for publication was Kan Liu.

low-coercive-force (LCF) magnets (AlNiCo, etc.), replacing total or partial high-coercive-force (HCF) magnets (NdFeB) in the conventional PMSMs. Because of the LCF magnets, the machine permanent magnet flux is able to be adjusted with magnetization or demagnetization current pulses while machine running (i.e., online magnetization manipulation). The LCF magnets will be demagnetized when the VFPM accelerates to high-speed-region. The machine voltage reduces, so that continuous flux-weakening current is eliminated. The losses caused by the flux-weakening control is then reduced. When the VFPM decelerates, the LCF magnets will be magnetized again to gain more back-EMF, increasing machine torque capabilities at the low-speed-region. With the magnetization state (MS) manipulation, the VFPM achieves wide-speed high-efficiency operation.

Recently, numerous papers have investigated design, analysis, and control of the VFPM [5], [6]. The VFPM can share

the same topology with the conventional PMSM. Therefore, surface-mounted VFPM [7], [8] and interior-mounted VFPM [9]–[12] have been proposed. The LCF magnets can be mounted on the stator as the stator permanent magnet VFPM [13], [14]. Efforts have been done to increase the overall efficiency [15], [16] and reduce the maximum magnetization current [17], [18], promoting the application of the VFPM.

The MS manipulation current control is a critical part of the VFPM control. Current control accuracy and manipulation speed are the two concerns. The magnetization current control accuracy determines the PM flux linkage control accuracy. The VFPM will benefit from fast manipulation speed, reducing manipulation losses and mechanical impact. Few papers have investigated how to increase the manipulation speed. A proper magnetization current trajectory should be designed to achieve the fast manipulation speed. Meanwhile, the current controller should have the capability to control the actual current tracking the designed trajectory. Linear trajectories have been studied in [19]. However, linear magnetization current trajectory causes voltage peaks that limit the maximum manipulation speed. A straight line stationary frame flux linkage trajectory method has been proposed in [20]. Sinusoidal current trajectories were implemented to reduce the voltage peaks, thereby increasing the manipulation speed. The negative sinusoidal current on q-axis generated brake torque, which leads to mechanical impact. The magnetization current controller shows two different approaches: the proportion-integration (PI) control method [21] and the dead-beat control method [22]. An improved feed-forward PI current controller has been proposed to increase the dynamic performance and control accuracy during the MS manipulation [19]. The dead-beat current control method significantly increases the current control dynamics. However, both the PI based method and the dead-beat based method are affected by the non-linearity in the magnetization.

The limited DC-link voltage is the cause of manipulation speed limitation. Therefore, this paper will propose an online MS manipulation current trajectory prediction and current control method, increasing the voltage utilization during the MS manipulation. The proposed method controls $i_q = 0$ during the MS manipulation to avoid brake torque. Meanwhile, the method predicts different i_d magnetization trajectories according to the machine operating conditions, i.e., the DC-link voltage and the machine speed. The prediction process is based on the dynamic VFPM mathematical model. The mathematical model reveals two different voltage types in the MS manipulation, which are the rotating voltage and the induction voltage. The rotating voltage and the induction voltage together contribute to the voltage requirement during the MS manipulation. The rotating voltage is an intrinsic voltage that has no relation to the manipulation speed. However, the rotating voltage is the key source for the q-axis current control. The induction voltage is generated by di/dt or $d\psi/dt$, which determines the MS manipulation speed. The proposed method is achieved by predicting the maximum induction voltage, which excludes the necessary
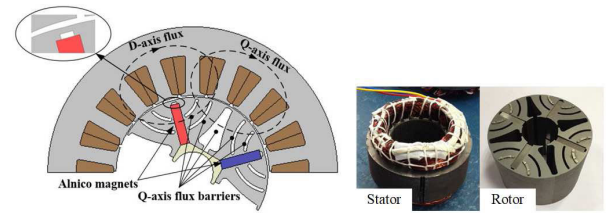

FIGURE 1. Topology and prototype of the studied VFPM.

TABLE 1. Specifications of the prototype VFPM.

Parameter	Value	Parameter	Value
Stator outer diameter	142 mm	Rated current	11 A
Stator inner diameter	75 mm	Rated torque	3.83 Nm
Rotor outer diameter	74 mm	Rated power	1.0 kW
PM thickness	4.5 mm	DC voltage	270 V
Maximum speed	6,000 rpm	Resistance	0.65 Ω
Average L_d	15.8 mH	Average L_q	13.5 mH

rotating voltage from the voltage source. The i_d manipulation trajectory is derived by the induction voltage using the inverse form of the machine model. A feed-forward current controller is implemented. The predicted rotating voltage and the predicted induction voltage are compensated in the standard PI regulators, in order to satisfy such high dynamic requirement in the current control. The proposed method uses the machine speed and the DC-link voltage in the prediction process, such that the method has self-adaptive capabilities in variable-speed and variable-voltage conditions. The proposed method was evaluated by various experiments. The experimental results show that the manipulation speed is increased by the high utilization rate of the DC-link voltage.

II. MACHINE AND MATHEMATICAL MODEL OF THE VFPM

A. SPECIFICATIONS OF THE STUDIED VFPM

A 4-poles and 18-slots spoke-type VFPM has been manufactured. Cross section, prototype stator and rotor are shown in Fig. 1. The LCF magnets, AlNiCo, are used as the source of the variable-flux. These magnets are tangentially magnetized, so that the flux is concentrated to achieve higher air-gap flux density. Flux barriers in the rotor create guidance for the d-axis armature flux, making the magnetization manipulation more easily and reducing the magnetization current amplitude. Specifications of the machine are listed in Table. 1.

The magnetization/demagnetization properties of the VFPM are closely related to the magnetization current i_d. The relation between the applied i_d and no-load PM flux linkage after the manipulation is shown in Fig. 2. The left side of the vertical axis is the demagnetization manipulations. The VFPM was magnetized to several levels (i.e., the points on the vertical axis), and then, the negative d-axis current was applied incrementally. The back-EMF was measured before and after each manipulation, so that the PM flux was calculated and the demagnetization curves were plotted. The right side of the vertical axis is the magnetization manipulation. The PM flux will not change until the applied magnetizing i_d
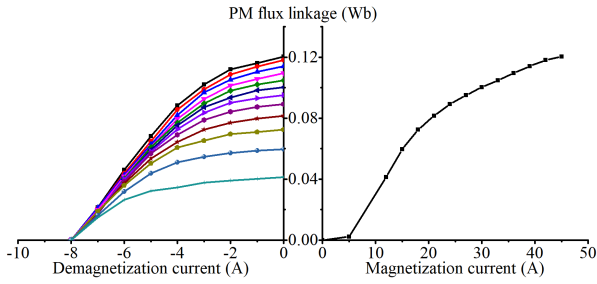
FIGURE 2. Relation between the machine PM flux and the applied magnetization current amplitude.

is larger than the magnetization current required at the current MS. Therefore, the magnetization property is expressed by a single curve. The maximum magnetization current is 45 A, achieving the maximum ψ_{PM} of 0.118 Wb. The prototype VFPM can be fully demagnetized with negative i_d of -8 A.

B. DYNAMIC MATHEMATICAL MODEL

The VFPM is a specific type of PM machines. Thus the mathematical model of the VFPM has a similar construction. The steady-state dq-axis voltage equation for the VFPM is expressed by (1) and (2):

$$u_d = Ri_d + L_d \frac{di_d}{dt} - \omega L_q i_q \qquad (1)$$

$$u_q = Ri_q + L_q \frac{di_q}{dt} + \omega L_d i_d + \omega \psi_{PM} \qquad (2)$$

Besides the normal operation, the VFPM has a distinctive operation, i.e., the magnetization manipulation. d-axis current pulses are injected, as a consequence, the PM flux linkage ψ_{PM} cannot be treated as constant value because the magnets are magnetized or demagnetized during the manipulations. The change in the PM flux causes induction voltage on d-axis, whose value cannot be neglected because the time span (dt) of a single magnetization manipulation is usually less than 100 ms. Therefore, the dynamic mathematical model for the magnetization manipulation is transferred to (3) and (4):

$$
\begin{aligned}
u_d &= u_{rd} + u_{iad} + u_{ifd} + u_{rfad} \\
&= Ri_d + \frac{d\psi_{ad}}{dt} + \frac{d\Psi_{PM}(i_d)}{dt} - \omega\psi_{aq} \qquad (3)
\end{aligned}
$$

$$
\begin{aligned}
u_q &= u_{rq} + u_{iaq} + u_{rfaq} + u_{rff} \\
&= Ri_q + \frac{d\psi_{aq}}{dt} + \omega\psi_{ad} + \omega\Psi_{PM}(i_d) \qquad (4)
\end{aligned}
$$

where u_{rd} and u_{rq} are resistive voltage on each axis. u_{iad} and u_{iaq} are the induction voltage caused by the change of armature flux linkage. u_{ifd} is the induction voltage caused by the PM flux change. u_{rfad} and u_{rfaq} are the cross-coupling rotating voltage created by the armature voltage. u_{rff} is the back-EMF. Considering the influences from machine non-linearity, the inductance value varies during the magnetization manipulations, so that the induction voltages and the rotating voltages are expressed with the flux linkage. The
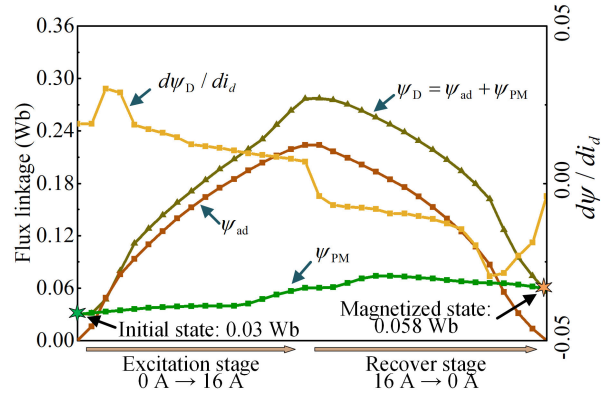

FIGURE 3. Flux variation in the 16 A magnetization from $\psi_{PM} = 0.03$ Wb.

PM flux linkage Ψ_{PM} are presented by the function of i_d, because the PM flux linkage is determined by the applied d-axis armature magnetic field.

III. VOLTAGE ANALYSIS OF THE MAGNETIZATION STATE MANIPULATION

A. ANALYSIS OF THE FLUX IN THE MS MANIPULATION

The voltage model contains the flux linkage amplitude $\psi(t)$ and the change rate of the flux linkage $d\psi(t)/dt$. The analysis on the voltage characteristics is transferred to the analysis on the flux variation during the MS manipulation. Finite element analysis was implemented to extract the detail flux, so that the non-linearity is considered. Because the magnetization current changes the working state of the Alnico magnets, distinctive magnet material BH curves should be configured in the FEA. Magnetization-Frozen FEA records the initial state of the Alnico magnets. Then the FEA method generates the BH curve to be configured, according to the experimentally measured BH loops and the manipulation specifications (e.g., manipulation current amplitude) [23]. A single MS manipulation has two stages. Excitation stage is to control i_d from normal operation to the magnetization command. Recover stage is to control i_d from the magnetization command to normal operation. The FEA is performed with discrete current of a complete MS manipulation, deriving the dq-axis flux linkage curves.

Fig. 3 presents a magnetization example, whose initial magnetization state is $\psi_{PM} = 0.03$ Wb. Discrete magnetization currents from $i_d = 0$ A via $i_d = 16$ A and finally return to $i_d = 0$ A were applied in the FEA. After the manipulation, the magnets were magnetized to a higher state, whose $\psi_{PM} = 0.058$ Wb. The total flux linkage ψ_D on d-axis is formed by the armature flux linkage ψ_{ad} and the PM flux linkage ψ_{PM}, as ($\psi_D = \psi_{ad} + \psi_{PM}$). The change rate of ψ_D to i_d ($d\psi_D/di_d$) is calculated by the discrete point in the figure. Material saturation effect and non-linear magnet properties contribute to the non-linear flux linkage and its change rate. Besides, flux in the excitation stage and the recover stage shows different behaviors.
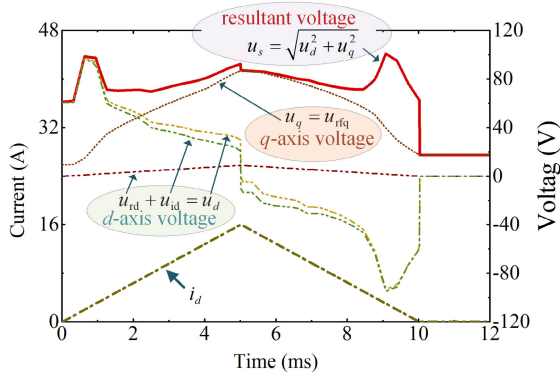
FIGURE 4. Voltage simulation in the 16 A magnetization with the slope of 3,200 A/s.

FIGURE 5. Simulated voltage and current waveform with different machine conditions.

B. VOLTAGE ANALYSIS WITH LINEAR MAGNETIZATION CURRENT TRAJECTORY

The FEA results reveal the relation between the flux and i_d. However, the voltage equations are based on the relation between flux and time. Therefore, the voltage equations (3) and (4) are re-written by:

$$u_d = u_{\mathrm{rd}} + u_{\mathrm{id}} + u_{\mathrm{rfd}}$$
$$= Ri_d + \frac{d\psi_{\mathrm{D}}(i_d)}{di_d}\frac{di_d}{dt} - \omega\psi_{\mathrm{aq}} \qquad (5)$$
$$u_q = u_{\mathrm{rq}} + u_{\mathrm{iaq}} + u_{\mathrm{rfq}}$$
$$= Ri_q + \frac{d\psi_{\mathrm{aq}}}{dt} + \omega\psi_{\mathrm{D}}(i_d) \qquad (6)$$

where $u_{\mathrm{id}} = u_{\mathrm{iad}} + u_{\mathrm{ifd}}$ is the total d-axis induction voltage. $u_{\mathrm{rfq}} = u_{\mathrm{rfaq}} + u_{\mathrm{rff}}$ is the total q-axis rotating voltage. The magnetization i_d can influence the flux on q-axis, because of the cross-saturation effect. This effect is ignored in this paper to simplify the analysis process.

The induction voltage u_{id} is calculated by the multiplication of the differential of the manipulation i_d trajectory and the corresponding flux change rate. Thus, different manipulation current trajectories have different voltage waveform. If the excitation stage and the recover stage are all linear trajectories, di_d/dt will be constant value. Fig. 4 presents the current and voltage waveform of the 16 A linear magnetization simulation. In the simulation, machine speed and manipulation time were 1,500 rpm and 10 ms respectively. Meanwhile, i_q was assumed zero in the simulation, such that q-axis voltage is composed by the rotating voltage u_{rfq}. Those voltages were calculated with the flux properties in Fig. 3 and the machine voltage equation (5) and (6). The resultant voltage u_s is the amplitude of the voltage vector, which appears three major voltage peaks in a complete magnetization manipulation. The first and the third voltage peaks happen when the manipulation i_d is relative small. The inductance value is higher because the machine saturation degree is lower when the magnetization i_d is small. Higher inductance value leads to higher induction voltage. The second voltage peak is caused by the rotating voltage on q-axis. This voltage is related to the amplitude of the flux on d-axis. Therefore,
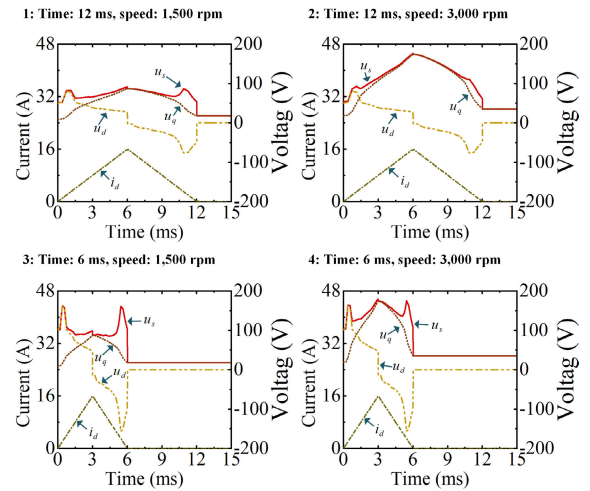
this voltage peak happens when i_d reaches its maximum value.

Fig. 5 compares the simulated voltage with different manipulation time (12 ms and 6 ms) and different machine speed (1,500 rpm and 3,000 rpm). Because the induction voltage peaks are determined by the current change rate (di_d/dt), faster manipulation speed creates higher induction voltage. The rotating voltage is the multiplication of machine speed and flux amplitude. Thus, higher machine speed makes the second voltage peak higher. Different manipulation time and machine speed together lead to distinctive voltage waveform shapes.

IV. TRAJECTORY PREDICTION AND CURRENT CONTROL

Faster magnetization speed benefits the VFPM system by shortening mechanical impact time and reducing losses in the manipulation. The commonly used linear trajectory manipulation current has limitation when the manipulation speed increases. The linear trajectory has constant di/dt, therefore the maximum induction voltage has to satisfy the limitation of the available voltage source. However, there is significant difference in the induction voltages, especially when the manipulation speed increases. As shown in Fig. 4 and Fig. 5, the peaks and valleys in the resultant voltage indicate that the voltage source is not able to be fully utilized with the linear trajectory. The target for increasing the voltage utilization changes the shape of the initial linear trajectory. Therefore, an online MS manipulation trajectory prediction method is proposed, aiming at increasing the voltage utilization.

A. METHOD FOR THE TRAJECTORY PREDICTION

The VFPM voltage equations show that the resultant voltage is created by the resistance voltage, the induction voltage, and the rotating voltage. Different from the induction voltage, the rotating voltage are created by the multiplication of the machine speed and the amplitude of the current or the flux
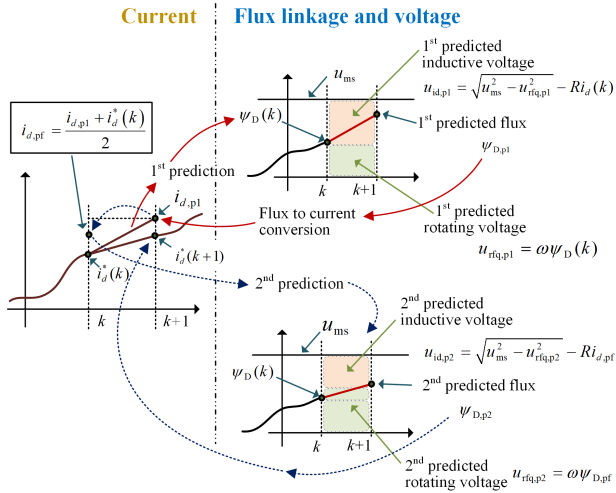
FIGURE 6. Trajectory prediction process in a single step.

linkage, which is not related to the manipulation speed. The concept of the proposed method is to predict the rotating voltage and resistance voltage first, and then the induction voltage occupies the remaining voltage source to increase the MS manipulation speed.

Because of the material non-linearity, the data in the flux model is used in the prediction to improve accuracy. The flux change under different magnetization current manipulation is distinctive, which affects the analysis and control. In this study, different manipulations have used the corresponding flux-current curve to overcome the effect from the flux change. The flux change in the excitation stage and the recover stage is also separated in the analysis and control. For example, the analysis on the 16 A magnetization uses the flux model in Fig. 3. With the flux linage and current operators $F_{(\psi)}$ and $F_{(i)}$ in (7) and (8), the value of i_d and the corresponding d-axis total flux linkage can be transformed to each other.

$$i_d = F_{(\psi)}\psi_D \tag{7}$$

$$\psi_D = F_{(i)}i_d \tag{8}$$

Fig. 6 presents the trajectory prediction process in a single step, and total prediction algorithm flow chart is presented in Fig. 7. The prediction method in a single step includes two predictions and a prediction feedback adjust. The 1st prediction uses the measured current $i_d(k)$ at time instance k and estimates the required rotating voltage $u_{\text{rfq,p1}}$ by:

$$u_{\text{rfq,p1}} = \omega\psi_D(k) = \omega F_{(i)}i_d(k) \tag{9}$$

then, the available d-axis inductive voltage $u_{\text{id,p1}}$ can be estimated by solving (5) and (6):

$$u_{\text{id,p1}} = \sqrt{u_{\text{ms}}^2 - u_{\text{rfq,p1}}^2} - Ri_d(k) \tag{10}$$

where $u_{\text{ms}} = u_{\text{DC}}/\sqrt{3}$ is the maximum phase voltage in the linear modulation region. Because i_q is controlled to be
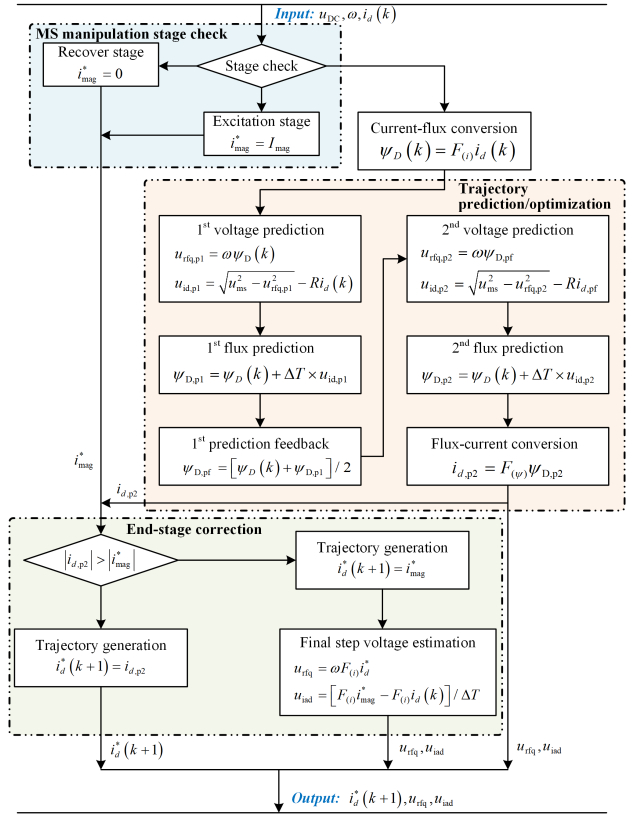

FIGURE 7. Flow chart of the proposed prediction method.

zero, the q-axis voltage only consists the rotating voltage u_{rfq}. The integration of the induction voltage equals the flux linkage change. Thus, the d-axis flux linkage $\psi_{D,\text{p1}}$ of next time instance is expressed in the differential form:

$$\psi_{D,\text{p1}} = \psi_D(k) + \Delta T \times u_{\text{id,p1}} \tag{11}$$

where ΔT is the sample interval in the discrete controller. If the predicted flux linkage $\psi_{D,\text{p1}}$ is larger than the initial flux linkage $\psi_D(k)$, i.e., the excitation stage in a magnetization manipulation, the rotating voltage will be increasing during a sample period. As a consequence, the available voltage for the induction voltage decreases. Therefore, ψ_D cannot reach the predicted level. A prediction feedback adjustment is developed to address this conflict. The middle value $\psi_{D,\text{pf}}$ between the initial flux $\psi_D(k)$ and the 1st predicted flux $\psi_{D,\text{p1}}$ is used for the estimation of the rotating voltage, as shown by:

$$\psi_{D,\text{pf}} = \frac{\psi_D(k) + \psi_{D,\text{p1}}}{2} \tag{12}$$

Similar to the 1st prediction, the 2nd predicted inductive voltage with the new $\psi_{D,\text{pf}}$ are calculated by:

$$u_{\text{rfq,p2}} = \omega\psi_{D,\text{pf}} \tag{13}$$

$$u_{\text{id,p2}} = \sqrt{u_{\text{ms}}^2 - u_{\text{rfq,p2}}^2} - Ri_{d,\text{pf}} \tag{14}$$

where $i_{d,\text{pf}}$ is derived by the flux $\psi_{D,\text{pf}}$. The 2nd flux prediction is calculated by the differential equation:
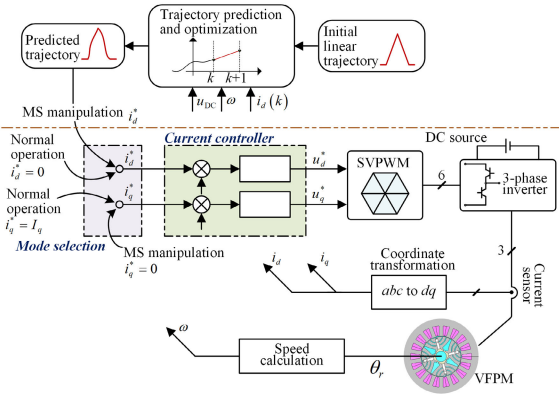
$$\psi_{D,\text{p2}} = \psi_D(k) + \Delta T \times u_{\text{id,p2}} \tag{15}$$

FIGURE 8. Trajectory prediction and field-oriented-control-based machine control system.

FIGURE 9. Feed-forward current controller inside the VFPM control system.

The corresponding *d*-axis current in the second prediction is then derived:

$$i_{d,\text{p2}} = F_{(\psi)}\psi_{D,\text{p2}} \tag{16}$$

$i_{d,\text{p2}}$ of the following control intervals form the MS manipulation trajectory. In the final control interval when the predicted trajectory approaches the targert value of each manipulation stages (i.e., the magnetization current command i^*_{mag} in the excitation stage, and 0 in the recover stage), not the full voltage source should be applied, in order to avoid current overshoot and MS manipulation error. An end-stage correction is proposed. if $i_{d,\text{p2}}$ is within the target value of each manipulation stage, the *d*-axis current command value is equal to the predicted $i_{d,\text{p2}}$. Otherwise, the command value is replaced by the manipulation target i^*_{mag}. Thus, the rotating voltage and the induction voltage can be estimated by:

$$u_{\text{rfq}} = \omega F_{(i)}i^*_{\text{mag}} \tag{17}$$

$$u_{\text{id}} = [F_{(i)}i^*_{\text{mag}} - F_{(i)}i_d(k)]/\Delta T \tag{18}$$

where i^*_{mag} is replaced by zero when the end-stage correction is in the recover stage.

B. SYSTEM IMPLEMENTATION AND FEED-FORWARD CURRENT CONTROLLER

The machine speed and the DC-link voltage are two of the major concerns in the MS manipulation trajectory prediction. The MS manipulation can be executed at different speeds. Moreover, the DC-link voltage can be variable in certain applications, e.g., electric vehicles using battery to feed the DC voltage. The battery voltage is variable due to discharge level and operating temperature. These two aspects affect the machine voltage and cause different manipulation trajectories. Therefore, a field-oriented-control-based machine control system with the online trajectory prediction is proposed in Fig. 8.

The DC-link voltage, the machine speed, and the *d*-axis current $i_d(k)$ are measured and used in the trajectory prediction algorithm, so that the predicted trajectory can be adjust according to different machine operating conditions. The trajectory is then transferred to the mode selection to determine
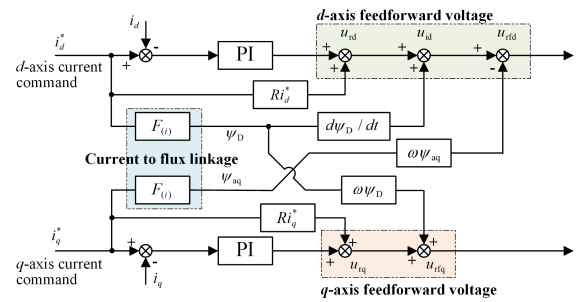
the VFPM whether is controlled in normal operation or the MS manipulation. During the MS manipulation, the *d*-axis current command is replaced by the predicted trajectory. i_q command is set by zero.

The increased current manipulation speed requires high-response current controller. Usually, PI gains in standard PI regulators are increased to satisfy the high bandwidth requirement. However, the higher PI gains can lead to current overshoot, deteriorating the control accuracy. Fig. 9 presents the improved current controller with feed-forward compensation. The feed-forward method compensates the required resistance voltage, induction voltage, and rotating voltage in the MS manipulation. The compensation voltages u_{ffd} and u_{ffq} on *dq*-axis are expressed by:

$$u_{\text{ffd}} = u_{\text{rd}} + u_{\text{id}} + u_{\text{rfd}} \tag{19}$$

$$u_{\text{ffq}} = u_{\text{rq}} + u_{\text{rfq}} \tag{20}$$

These compensated voltages have been already derived in the trajectory prediction algorithm. Influences from parameter non-linearity is eliminated because the trajectory prediction has considered the non-linear relation between flux and current. The mathematical expression for the current controller is shown by:

$$u^*_x = k_{\text{p}x}(i^*_x - i_x) + k_{\text{i}x}\int(i^*_x - i_x)dt + u_{\text{ff}x} \tag{21}$$

where the subscript *x* stands for the *d*- or *q*-axis. k_p and k_i are the proportional and integral gain respectively. With the feed-forward controller, the tuning load of the PI regulators decreases. A fixed PI gain can achieve high-response and accurate trajectory tracking performance.

V. SIMULATION VERIFICATION

The simulation is achieved by solving the voltage equations with the given current waveform. The 16 A magnetization manipulation was simulated, which is the magnetization from $\psi_{\text{PM}} = 0.03$ Wb to $\psi_{\text{PM}} = 0.058$ Wb. The flux-current model was embed in the model, so that influence from parameter non-linearity was considered.

This simulation was performed under the condition of $u_{\text{DC}} = 270$ V ($u_{\text{ms}} = 156$ V) and 2,000 rpm. Fig. 10 presents current and voltage waveform of the linear trajectory and the predicted trajectory. Manipulation speed of the linear
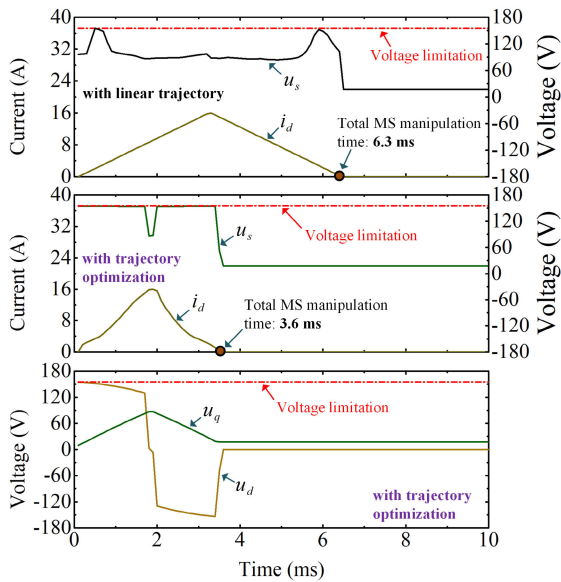
FIGURE 10. Simulated 16 A magnetization waveform of the linear trajectory and the predicted trajectory.

FIGURE 11. Flux data in the 26 A magnetization.

FIGURE 12. Online 16 A magnetization waveform.

FIGURE 13. Online 26 A magnetization waveform.

trajectory is limited by the two voltage peaks, which is caused by the induction voltage and should not exceed the voltage limitation. The total MS manipulation time of the linear trajectory is 6.3 ms, including the whole excitation and recover stages.

Total manipulation time of the predicted trajectory is 3.6 ms, which reduces by 43%. The i_d waveform presents a non-linear shape. The phase voltage amplitude approaches the voltage limitation in the whole manipulation, excluding when i_d nears the manipulation target. Such local voltage change successfully avoids i_d exceeding the manipulation target of 16 A. The third row in Fig. 10 exhibits the dq-axis voltage waveform with the predicted trajectory. u_q is determined by the rotating voltage. d-axis voltage successfully occupies the remaining voltage source. The enlarged d-axis induction voltage boosts the MS manipulation speed.

VI. EXPERIMENTAL VERIFICATION
The proposed method was tested on the prototype VFPM. The VFPM was fed by a three-phase half-bridge inverter. The DSP TMS320F28335 from TI was implemented for the execution of the proposed method. Current sampling frequency and switching frequency were the same 10 kHz. Control variables, e.g., i_d, i_q, and feed-forward voltages, were displayed by the digital-to-analog (DA) conversion on the control board. A ScopeCorder from Yokogawa recorded phase currents, voltage, and the control variables. The DA has the output range of 0 V to 5 V. The conversion ratio between the actual value and the DA output is listed in the experimental figures. The tested machine was controlled in the speed-command mode. $i_d = 0$ control was selected in normal operations. During magnetization manipulation, the speed-loop was disconnected. i_q command was set by zero. Because
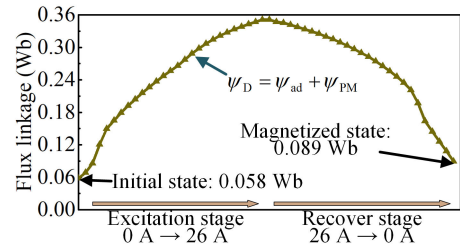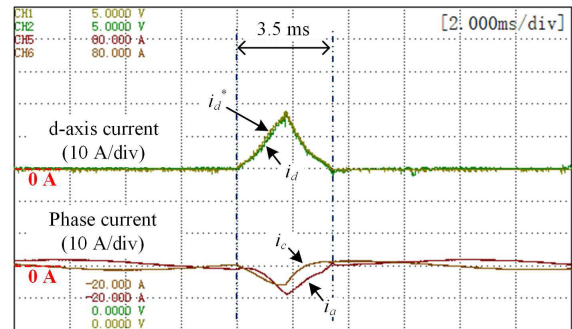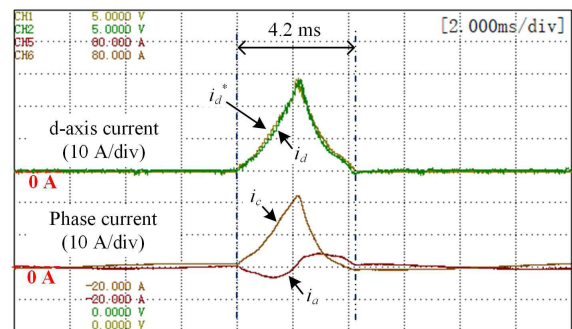
the manipulation period is short (within several milliseconds), the speed variation during the manipulation can be neglected.

A. ONLINE MAGNETIZATION EVALUATION
The machine was controlled at 2,000 rpm. The DC-link voltage was set by 270 V. The initial MS of the machine was $\psi_{PM} = 0.03$ Wb. A magnetization current of 16 A was applied to increase the MS to $\psi_{PM} = 0.058$ Wb. Then, another magnetization current of 26 A was applied, increasing the MS to $\psi_{PM} = 0.089$ Wb. The flux data used in the 26 A magnetization manipulation is shown in Fig. 11. The experimental waveform was shown in Fig. 12 and Fig. 13, respectively. i_d tracked the predicted trajectory with high accuracy. The manipulation time of the 16 A magnetization and the 26 A magnetization was 3.5 ms and 4.2 ms, respectively. The manipulation time of the 16 A magnetization approximated the time (3.6 ms) in the simulation part. Because the rotating voltage on the q-axis is higher in the
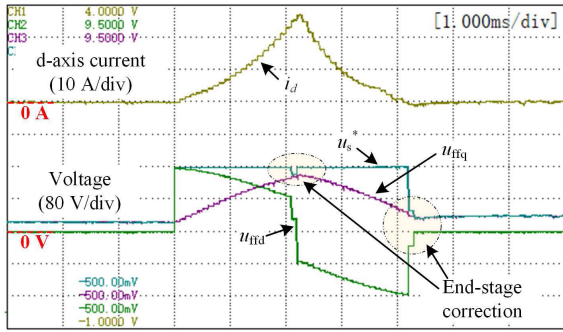
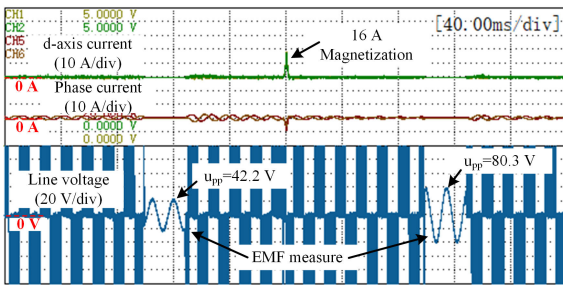**FIGURE 14.** Feed-forward voltages in the 26 A magnetization.

FIGURE 15. Back-EMF measurement in the 16 A magnetization.

FIGURE 16. Back-EMF measurement in the 26 A magnetization.

FIGURE 17. Successive 16 A magnetization at different speeds.

26 A magnetization, the manipulation time of the 26 A magnetization was larger than the time in the 16 A magnetization.

Fig. 14 shows the feed-forward voltages of the 26 A magnetization. The total compensated phase voltage showed a high utilization of the phase voltage limitation (156 V of the 270 V DC-link voltage). The voltage drops in the end-stage corrections successfully controlled i_d not exceeding the magnetization command.

B. EVALUATION OF THE MS MANIPULATION ACCURACY

The machine back-EMF was measured before and after a magnetization manipulation. The PWM pulses were blocked for a short time period, so that the machine speed changes little. The line voltage equals the line back-EMF during the power interruption. Therefore, the back-EMF was directly measured by the voltage probes. Fig.15 and Fig.16 present the experiments on the 16 A magnetization and the 26 A magnetization, respectively. After a 16 A magnetization, the line back-EMF increased to 80.3 V. Because the machine was controlled at 2,000 rpm, the PM flux linkage equaled 0.056 Wb, showing a 0.002 Wb (3.4%) error with the manipulation target 0.058 Wb. The error in the measurement of the magnetization properties (Fig. 2) leads to the magnetization manipulation error. The line back-EMF after the 26 A magnetization was 124.5 V. Therefore, the MS of the 26 A magnetization was 0.086 Wb. The MS control error in this manipulation was 0.003 Wb (3.4%), with the target of 0.089 Wb. Both the two manipulations show good accuracy. The error in the measurement of the magnetization properties (Fig. 2) leads to the magnetization manipulation error.
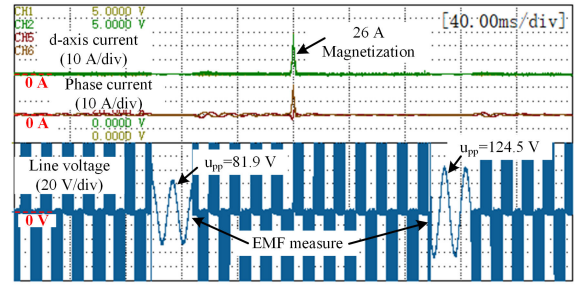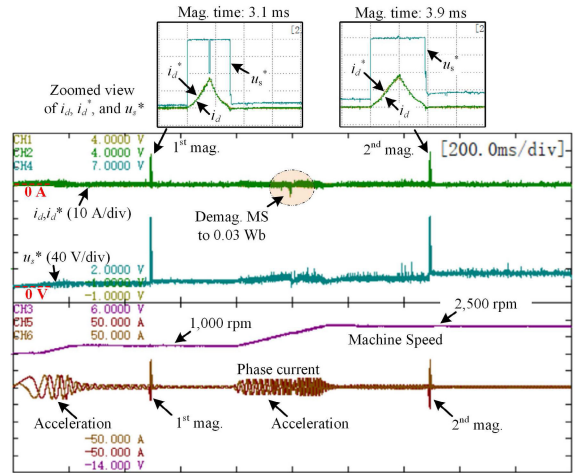
C. MS MANIPULATION AT DIFFERENT MACHINE SPEEDS

The same magnetization manipulation was tested successively at different speeds, such that the self-adaptive capability of the proposed method can be evaluated. Fig. 17 presents the experimental waveform. The initial MS of the VFPM was 0.03 Wb. The machine speed was controlled in a ladder form acceleration. During the two accelerations, the phase current was regulated increasing to generate the required traction torque for the accelerations. The same 16 A magnetization was manipulated twice when the machine speed reached 1,000 rpm and 2,500 rpm, respectively. Between the two magnetizations, a -5.8 A demagnetization current was applied to demagnetize the machine to the initial MS of 0.03 Wb, so that the second 16 A magnetization manipulation could start with the same MS. The zoomed view of the two manipulations compared the *d*-axis current and its command trajectories. Both the two i_d waveforms tracked the predicted trajectories i_d^* with high accuracy. The *dq*-axis resultant compensated voltage amplitude u_s^* was also plotted in the zoomed view. Both the two u_s^* waveforms exhibited highly saturated straight lines, meaning the high utilization level (156 V u_{ms} under 270 V u_{DC}) during the whole magnetization. Time duration of the two manipulations was 3.1 ms at lower speed and 3.9 ms at higher speed, respectively. Because the rotating voltage is larger at higher
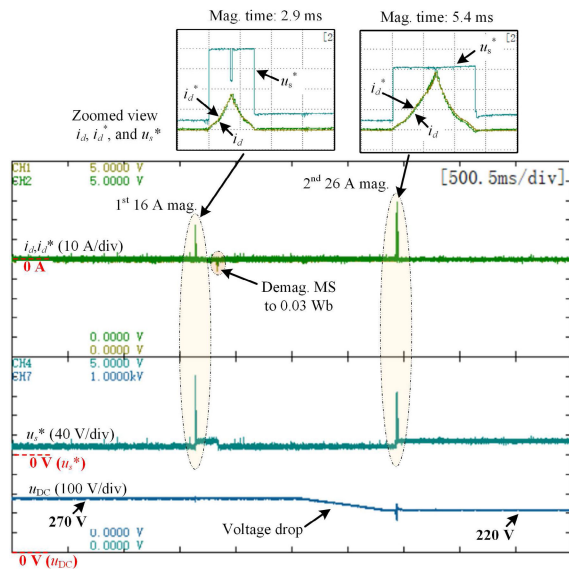
FIGURE 18. Successive magnetization with variable DC-link voltage.

machine speed, the available voltage for the *d*-axis induction voltage is limited. Therefore, the magnetization current at higher machine speed is manipulated at a slower rate.

D. MS MANIPULATION WITH DIFFERENT DC-LINK VOLTAGE

The machine speed was controlled at 1,500 rpm in this experiment. The initial MS was 0.03 Wb. The first 16 A magnetization was manipulated under the DC-link voltage of 270 V. After the first magnetization was finished, the machine was demagnetized to the initial state of 0.03 Wb. Then, the DC-link voltage was adjusted to 220 V, and the second 26 A magnetization was executed. Fig. 18 presents the voltage and current waveform. The zoomed view showed the details of each manipulation. The level of the compensated voltage u_s^* was lower in the second magnetization because of the reduced DC-link voltage. But, u_s^* still exhibited the high utilization rate under the different DC-link voltages.

All the magnetization current i_d coincided with its predicted trajectories in the above experimental results. The effectiveness of the proposed method was verified under various machine speed, different DC-link voltage, and different magnetization current

VII. CONCLUSION

This paper proposed an online current trajectory prediction and control method for the magnetization current in a variable-flux permanent magnet machine. The proposed method achieved a high utilization rate within the whole magnetization manipulation, thereby increasing the manipulation speed. The trajectory can be adjusted online with different machine conditions because the machine speed and the DC-link voltage are the key index in the proposed method. This method decouples the two critical voltages in the magnetization manipulation, which are the rotating

voltage and the induction voltage. The rotating voltage contributes to the *q*-axis current control. The induction voltage is the source of the magnetization current control. The prediction method maximizes the induction voltage while remaining the necessary voltage for the *q*-axis current. Flux non-linearity is considered in the algorithm, such that high control accuracy is achieved in the highly-saturated magnetization manipulations.

REFERENCES

[1] G. Hong, T. Wei, and X. Ding, "Multi-objective optimal design of permanent magnet synchronous motor for high efficiency and high dynamic performance," *IEEE Access*, vol. 6, pp. 23568–23581, 2018.
[2] H. Chen and C. H. T. Lee, "Parametric sensitivity analysis and design optimization of an interior permanent magnet synchronous motor," *IEEE Access*, vol. 7, pp. 159918–159929, 2019.
[3] V. Ostovic, "Memory motors," *IEEE Ind. Appl. Mag.*, vol. 9, no. 1, pp. 52–61, Jan. 2003.
[4] K. Sakai, K. Yuki, Y. Hashiba, N. Takahashi, and K. Yasui, "Principle of the variable-magnetic-force memory motor," in *Proc. Int. Conf. Electr. Mach. Syst.*, Nov. 2009, pp. 1–6.
[5] H. Jia, W. Xinjian, and S. Zechang, "Variable flux memory motors: A review," in *Proc. IEEE Conf. Expo Transp. Electrific. Asia–Pacific (ITEC Asia–Pacific)*, Aug. 2014, pp. 1–6.
[6] H. Yang, H. Lin, and Z. Q. Zhu, "Recent advances in variable flux memory machines for traction applications: A review," *CES Trans. Electr. Mach. Syst.*, vol. 2, no. 1, pp. 34–50, Mar. 2018.
[7] J.-M. Kim, J.-Y. Choi, K.-S. Lee, and S.-H. Lee, "Design and analysis of surface-mounted-type variable flux permanent magnet motor for wide-speed range applications," *IEEE Trans. Magn.*, vol. 51, no. 11, pp. 1–4, Nov. 2015.
[8] J.-M. Kim, J.-Y. Choi, S.-H. Lee, and S.-M. Jang, "Characteristic analysis and experiment of surface-mounted type variable-flux machines considering magnetization/demagnetization based on electromagnetic transfer relations," *IEEE Trans. Magn.*, vol. 50, no. 11, pp. 1–4, Nov. 2014.
[9] A. Sun, J. Li, R. Qu, J. Chen, and H. Lu, "Rotor design considerations for a variable-flux flux-intensifying interior permanent magnet machine with improved torque quality and reduced magnetization current," in *Proc. IEEE Energy Convers. Congr. Exposit. (ECCE)*, Sep. 2015, pp. 784–790.
[10] M. Ibrahim, L. Masisi, and P. Pillay, "Design of variable-flux permanent-magnet machines using alnico magnets," *IEEE Trans. Ind. Appl.*, vol. 51, no. 6, pp. 4482–4491, Nov. 2015.
[11] H. Hua, Z. Q. Zhu, A. Pride, R. Deodhar, and T. Sasaki, "Comparative study of variable flux memory machines with parallel and series hybrid magnets," in *Proc. IEEE Energy Convers. Congr. Exposit. (ECCE)*, Oct. 2017, pp. 3942–3949.
[12] A. Athavale, K. Sasaki, B. S. Gagas, T. Kato, and R. D. Lorenz, "Variable flux permanent magnet synchronous machine (VF-PMSM) design methodologies to meet electric vehicle traction requirements with reduced losses," *IEEE Trans. Ind. Appl.*, vol. 53, no. 5, pp. 4318–4326, Sep. 2017.
[13] H. Yang, Z. Q. Zhu, H. Lin, and S. Lyu, "Comparative study of hybrid PM memory machines having Single- and dual-stator configurations," *IEEE Trans. Ind. Electron.*, vol. 65, no. 11, pp. 9168–9178, Nov. 2018.
[14] X. Zhu, Z. Xiang, L. Quan, W. Wu, and Y. Du, "Multimode optimization design methodology for a flux-controllable stator permanent magnet memory motor considering driving cycles," *IEEE Trans. Ind. Electron.*, vol. 65, no. 7, pp. 5353–5366, Jul. 2018.
[15] B. Gagas, T. Fukushige, N. Limsuwan, C.-Y. Yu, K. Akatsu, and R. D. Lorenz, "Suggested design space in a PMSM parameter plane for variable flux machines," in *Proc. Int. Electric Mach. Drives Conf.*, May 2013, pp. 549–556.
[16] A. Athavale, K. Sasaki, B. S. Gagas, T. Kato, and R. D. Lorenz, "Variable flux permanent magnet synchronous machine (VF-PMSM) design to meet electric vehicle traction requirements with reduced losses," in *Proc. IEEE Energy Convers. Congr. Exposit. (ECCE)*, Sep. 2016, pp. 1–8.
[17] Y. Lu, J. Li, R. Qu, A. Sun, and H. Fang, "A method to improve torque density and reduce magnetization current in a variable-flux flux-intensifying interior permanent magnet machine," in *Proc. IEEE Vehicle Power Propuls. Conf. (VPPC)*, Oct. 2016, pp. 1–5.

[18] M. Ibrahim, L. Masisi, and P. Pillay, "Design of variable flux permanent-magnet machine for reduced inverter rating," *IEEE Trans. Ind. Appl.*, vol. 51, no. 5, pp. 3666–3674, Sep. 2015.

[19] J. Chen, J. Li, and R. Qu, "Analysis, modeling, and current trajectory control of magnetization state manipulation in variable-flux permanent magnet machines," *IEEE Trans. Ind. Electron.*, vol. 66, no. 7, pp. 5133–5143, Jul. 2019.

[20] B. S. Gagas, K. Sasaki, T. Fukushige, A. Athavale, T. Kato, and R. D. Lorenz, "Analysis of magnetizing trajectories for variable flux PM synchronous machines considering voltage, high-speed capability, torque ripple, and time duration," *IEEE Trans. Ind. Appl.*, vol. 52, no. 5, pp. 4029–4038, Sep. 2016.

[21] L. Masisi, M. Ibrahim, and P. Pillay, "Control strategy of a variable flux machine using AlNiCo permanent magnets," in *Proc. IEEE Energy Convers. Congr. Exposit. (ECCE)*, Sep. 2015, pp. 5249–5255.

[22] A. Athavale, D. J. Erato, and R. D. Lorenz, "Enabling driving cycle loss reduction in variable flux PMSMs via closed-loop magnetization state control," *IEEE Trans. Ind. Appl.*, vol. 54, no. 4, pp. 3350–3359, Jul. 2018.

[23] J. Chen, J. Li, R. Qu, and M. Ge, "Magnet-Frozen-Permeability FEA and DC-biased measurement for machine inductance: Application on a variable-flux PM machine," *IEEE Trans. Ind. Electron.*, vol. 65, no. 6, pp. 4599–4607, Jun. 2018.

JUNHUA CHEN (Member, IEEE) received the B.E.E. and Ph.D. degrees in electrical engineering from the Huazhong University of Science and Technology, Wuhan, China, in 2013 and 2018, respectively.

He is currently a Postdoctoral Fellow with the Huazhong University of Science and Technology. His research interests include control of PM machines and power electronics.

HAIYANG FANG (Member, IEEE) was born in Hubei, China. He received the B.M.E. degree in mechanical engineering and the Ph.D. degree in electrical engineering from the Huazhong University of Science and Technology, Wuhan, China, in 2013 and 2018, respectively. He is currently a Postdoctoral Fellow with the Huazhong University of Science and Technology. His research interests include mechanical design and vibro-acoustic analysis of electrical machines.

RONGHAI QU (Fellow, IEEE) was born in China. He received the B.E.E. and M.S.E.E. degrees in electrical engineering from Tsinghua University, Beijing, China, in 1993 and 1996, respectively, and the Ph.D. degree in electrical engineering from the University of Wisconsin–Madison, in 2002.

In 1998, he joined the Wisconsin Electric Machines and Power Electronics Consortiums as a Research Assistant. He became a Senior Electrical Engineer with Scott Fetzer Company, Northland, in 2002. Since 2003, he has been a Senior Electrical Engineer with the Electrical Machines and Drives Laboratory, General Electric (GE) Global Research Center, Niskayuna, NY, USA. Since 2010, he has been a Professor with the Huazhong University of Science and Technology, Wuhan, China. He has authored over 120 published technical articles. He holds over 50 patents/patent applications.

Dr. Qu is a Full Member of the Sigma Xi. He was a recipient of several awards from the GE Global Research Center, including the Technical Achievement and Management Awards, the 2003 and 2005 Best Paper Awards, and the Third Prize from the Electric Machines Committee of the IEEE Industry Applications Society at the 2002 and 2004 IAS Annual Meeting.

• • •